ORNL/TM--9727

DE86 001366

Engineering Physics and Mathematics Division

THE HIGH ENERGY TRANSPORT CODE HETC*

T. A. Gabriel

*Published in the Proceedings
of the LEP Experimenters' Workshop
on Shower Simulation, CERN, Geneva,
Switzerland, January 29-31, 1985.

Date of Issue: September 1985

Research sponsored by
U.S. Dept. of Energy
Office of High Energy
and Nuclear Physics

Prepared by the
Oak Ridge National Laboratory
Oak Ridge, Tennessee 37831
operated by Martin Marietta Energy Systems, Inc.
for the U.S. DEPARTMENT OF ENERGY
under Contract No. DE-AC05-840R21400

ACKNOWLEDGMENT

The author wishes to thank Drs. R. G. Alsmiller, Jr. and T. W. Armstrong for their extensive help in preparing this manuscript.

TABLE OF CONTENTS

Introduction	1
Physics Within HETC	1
Charged–Particle Energy Loss	1
Multiple Coulomb Scattering	2
Charged–Pion Decay in Flight	2
Charged–Pion Decay and Capture at Rest	2
Neutral–Pion Decay	2
Muon Decay in Flight and at Rest	2
Elastic Nuclear Collisions	3
Inelastic Hydrogen Collisions	3
Inelastic Nuclear Collisions	3
An Application Using HETC	7
REFERENCES	14

ABSTRACT

The physics contained in the High Energy Transport Code (HETC), in particular the collision models, are discussed. An application using HETC as part of the CALOR code system is also given.

THE HIGH ENERGY TRANSPORT CODE, HETC*

T. A. Gabriel
Oak Ridge National Laboratory, Oak Ridge, Tennessee 37831 USA

Introduction

Any high-energy transport code must incorporate several basic features if the results obtained from this code are to be reliable and realistic. These features include nuclear elastic and inelastic interactions, decay, and atomic interactions (ionization and excitation effects and occasionally, Coulomb scattering). HETC[1] contains all of these features and more and has for many years been a benchmark code for simulating particle cascades.

HETC simulates the particle cascade by using Monte Carlo techniques to compute the trajectories of the primary particle and the secondary particles produced in nuclear collisions. The particles considered by HETC (protons, neutrons, π^+, π^-, μ^+, or μ^-) may be arbitrarily distributed in angle, energy, and space. HETC uses the combinatorial geometry package described in another paper at this conference so virtually arbitrary geometries are allowed. Each particle in the cascade is followed until it eventually disappears by escaping from the geometric boundaries of the system, undergoes nuclear collision or absorption, comes to rest due to energy losses from ionization and excitation of atomic electrons, or, in the case of pions and muons, decays. Photons produced in the cascade from π° decays or from deexcitation gamma rays are not transported, but information relating to the photons is stored for transport by codes such as EGS.[2] A complete cascade history tape is provided by HETC so that analysis of specific problems can be performed. The methods used in HETC to treat particular physical processes will now be described.

Physics Within HETC

Charged-Particle Energy Loss

The energy loss of protons, charged pions, and muons due to the excitation and ionization of atomic electrons is treated using the well-established stopping power formula[3] based on the continuous slowing-down approximation. Range straggling is taken into account. The density-effect correction to the stopping-power formula is calculated using the asymptotic form of the correction.[4]

Range-energy tables for each material in the system are computed for protons. These same tables are used for charged pions and muons by making use of scaling relations.[5]

Multiple Coulomb Scattering

Multiple Coulomb scattering of primary particles is treated using Fermi's joint distribution function for angular and lateral spread and Rutherford's single-scattering cross-section formula.[3] The scattering is implemented by arbitrarily dividing the charged-particle range into subtrajectories (nominally set equal to one-tenth of the range) and applying the lateral-spread and angle-change corrections due to multiple Coulomb scattering at the end points of the subtrajectories.[6] HETC is presently programmed to allow multiple Coulomb scattering only for the primary charged particles.

Charged-Pion Decay in Flight

Charged-pion decay in flight is taken into account using the known pion lifetime. The energy and angular distribution of the muon is obtained by assuming that the pion decay is isotropic in the rest frame of the pion and by using the Lorentz transformation to transform the distribution from the pion rest frame into the laboratory system. The neutrino produced is not considered.

Charged-Pion Decay and Capture at Rest

A positively charged pion which comes to rest is assumed to decay immediately into a positively charged muon and a neutrino, and the energy and angular distribution of the muon is obtained in the same manner as discussed above for pion decay in flight. A negatively charged pion which comes to rest may either decay or be captured by a nucleus, depending on the material atom density. Accordingly, an option is provided in HETC as to the treatment of all π^--mesons reaching the cutoff energy. If decay is specified, all π^--mesons reaching the cutoff energy are assumed to decay immediately into negatively charged muons and neutrinos. If capture is selected, all π^- mesons reaching the cutoff energy are forced to undergo nuclear capture, and the energy and angular distribution of the particles produced as a result of this capture is obtained using the intranuclear-cascade-evaporation model (see later section). It has previously been shown that this model describes the π^- capture process quite well.[7]

Neutral-Pion Decay

The neutral pion is very unstable and for practical purposes may be assumed to decay into two photons at its point of origin. Accordingly, HETC does not transport neutral pions, although the energy, direction, and spatial point of the neutral pions produced are included as part of the output.

Muon Decay in Flight and at Rest

Muons are unstable and will decay into electrons or positrons, (depending on the charge of the muons) and neutrinos. Muon decay in flight is taken into account using the known muon lifetime, and muons which come to rest are assumed to decay immediately. No information for the electrons, positrons, or neutrinos from muon decay is calculated.

Elastic Nuclear Collisions

Elastic collisions of protons and pions with all nuclei other than hydrogen are neglected at all energies. Elastic collisions by neutrons with nuclei other than hydrogen at energies above the neutron cutoff energy (usually 20 MeV) is optional in HETC, and if the option is chosen, requires the input of elastic scattering cross section data (σ_s and $d\sigma_s/d\Omega$).

Elastic collisions of protons, neutrons and charged pions with hydrogen nuclei are treated using experimental data and/or parametric fits to experimental data.[8]

Inelastic Hydrogen Collisions

Pion production is based on the isobar model of Sternheimer and Lindenbaum.[9] The particie cross sections are based on experimental data and/or models. Only single- and double-pion production in nucleon-hydrogen collisions and single-pion production in pion-nucleon collisions are accounted for. This model is used for energies up to 3.5 GeV for neutrons and protons and up to 25 GeV for charged pions.

Nonelastic nucleon collisions and charged-pion collisions with hydrogen nuclei at energies above 3.5 GeV and 2.5 GeV, respectively, are treated by using the calculational methods of Ref. 8 . This method utilizes experimental data for the total nonelastic n-p, p-p, π^+-p, and π^--p cross sections and the analytic fits to experimental data by Ranft and Borek[8] to determine the particle type, energy, and direction of the collision products. Special provisions are made to insure that energy and nucleons are conserved for each collision.

Inelastic Nuclear Collisions

The intranuclear-cascade evaporation concept of particle-nucleus interaction as implemented by Bertini[10] is used to determine the effect of particle-nucleus collisions below 3.5 GeV for nucleons and 2.5 GeV for charged pions. This Monte Carlo program has been used for a variety of calculations and has been shown to agree well with many experimental results in the energy range below 3 GeV. The underlying assumption of the intranuclear-cascade model is that particle-nuclear interactions can be treated as a series of two-body collisions within the nucleus and that the locations of the collision and resulting particles from the collision governed by experimental and/or theoretical particle-particle total- and differential-cross-section data. The types of particle collisions included in the calculation are elastic, inelastic, and charge exchange.

This model incorporates the diffuseness of the nuclear edge, the Fermi motion of the bound nucleons, the exclusion principle, and a local potential for nucleons and pions.

The density of the neutrons and protons within the nucleus (which is used with the total-cross-section data to determine interaction locations) is determined from the experimental data of Hofstadter.[11] The Hofstadter density profile for ^{16}O is given in Fig. 1(a) along with the three-region configuration used in the calculation which approximates the continuous density

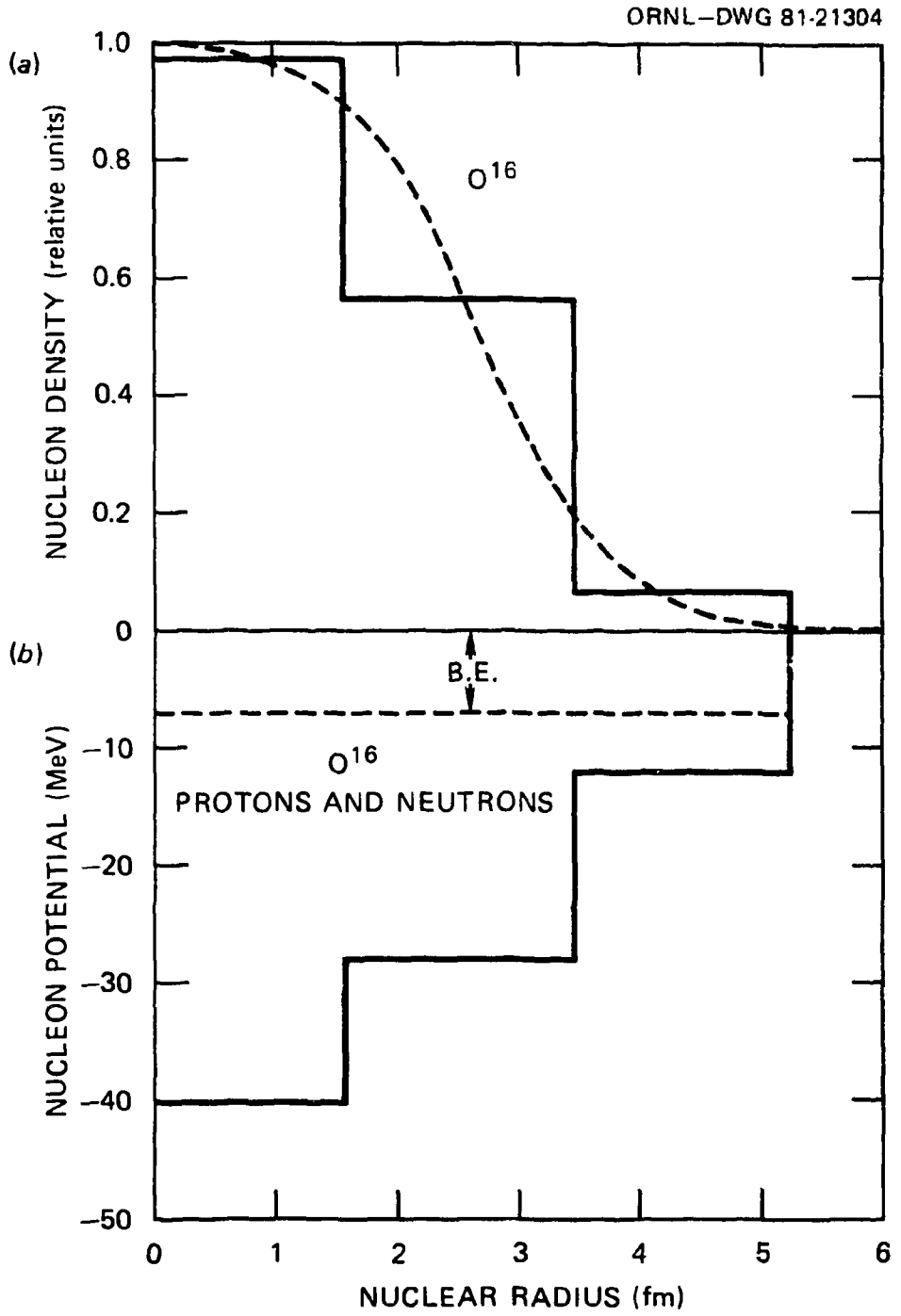

Fig. 1. (a) A comparison between the Hofstadter data (—) for ^{16}O and the nuclear cascade model. (b) Nucleon potential vs. nuclear radius for ^{16}O. B.E. is the fixed binding energy of the most loosely bound nucleon (7 MeV).

variation. Nuclear potentials are determined from these three density profiles by using a zero-temperature Fermi distribution. The total well depth is then defined as the Fermi energy plus 7 MeV (which represents the average binding energy of the most loosely bound nucleon). The well potentials for ^{16}O are given in Fig. 1(b).

Following the intranuclear-cascade phase of the calculation, there is excitation energy left in the nucleus due to particle capture and holes produced in the Fermi sea. This residual energy is treated by using an evaporation model. The particles allowed during evaporation include protons, neutrons, d, T, ^3He, and α.

An extrapolation model determines the energy, angle, and multiplicity of the products from inelastic nucleon-nucleus and pion-nucleus collisions at higher energies ($\geq$ 3 GeV).[12] This extrapolation method employs the particle-production data obtained from an intranuclear-cascade calculation for intermediate-energy ($\sim$ 3 GeV) nucleon-nucleus and pion-nucleus collisions, together with energy, angle, and multiplicity scaling relations that are consistent with the sparse experimental data available for high-energy collisions, to estimate the particle production for higher energy ($\geq$ 3 GeV) collisions. This extrapolation method is applicable to only those particles produced in the cascade phase of the collision; particle emission resulting from the deexcitation of the residual nucleus that is left after the emission of the cascade particles is determined by performing an evaporation calculation in the same manner as for nonscaled collisions.

Although the extrapolation model used is described in detail in Ref. 12, a synopsis of the method will be given here for completeness. Consider a particle-nucleus collision by a particle (nucleon or charged pion) with energy E_o and a collision with the same nucleus by the same type of particle but at some higher energy E_o', where E_o and E_o' are kinetic energies in the laboratory system. The extrapolation model for relating the products from the "slow" collision at E_o to the products from the "fast" collision at E_o' is based upon the following four assumptions:

(a) The total nonelastic cross section above E_o is independent of the energy of the incident particle, i.e., $\sigma(E_o') = \sigma(E_o)$.

(b) The residual excitation energy after the fast and slow collisions is the same.

(c) The transverse momentum in the center-of-momentum (CM) system of each produced particle is assumed to be the same in the fast and slow collisions, i.e.,

$$P_{ci}' \sin \Theta_{ci}' = P_{ci} \sin \Theta_{ci}$$

where c denotes CM quantities, i denotes the particle type (neutron, proton, π^+, π^o, or π^-), P is the momentum, and Θ is the polar angle with respect to the direction of the incident particle. To make this transformation unique, it is further assumed that the sign of $\cos \Theta_{ci}'$ is the same as the sign of $\cos \Theta_{ci}$.

(d) To relate the energies of the particles produced in the fast and slow collisions, the following scaling relation for kinetic energies is postulated for the CM system:

$$E'_{ci}/E'_{co} = E_{ci}/E_{co}.$$

By using the above assumptions, conservation of energy in the CM system for the fast and slow collisions, conservation of energy and momentum for the fast collision in the laboratory system, and the results of the intranuclear cascade calculation at E_o, the energy and direction of each emitted particle and the excitation energy, recoil energy, charge, and mass of the residual nucleus are determined for collisions at E'_{co}.† Further particle emission due to the deexcitation of the residual nucleus is obtained by performing an evaporation calculation as mentioned earlier. An intranuclear-cascade-evaporation-evaporation calculation is performed by HETC for each high-energy ($> E_o$) nonelastic nuclear collision that occurs during the transport calculation. In HETC E_o is fixed at 3.5 GeV for nucleon-nucleus collisions and results obtained with 2.5 GeV for pion-nucleus collisions since these are the maximum energies allowed by the intranuclear-cascade routines. Calculated results obtained with the extrapolation method are compared in Ref. 12 with experimental data for protons in the energy range from 12.5 to 70 GeV incident on Be, Al, Pb, and W nuclei.

There are several favorable features of the intranuclear-cascade-evaporation-evaporation model for treating nuclear interactions that are particularly noteworthy:

1. Energy and momentum are conserved in the laboratory system at each individual collision.

2. The method is completely parameter-free. Also, the basic experimental data needed are free particle-particle cross sections up to $\sim$ 3 GeV used in the intranuclear cascade, and these cross sections are relatively well known.

3. The produced particle spectra are obtained over the entire allowable energy range. This is in contrast to most other calculational methods for treating high-energy collisions in which the particle spectra below $\sim$100 MeV are either extremely approximate or neglected.

4. The charge and mass of the residual nucleus are obtained after each collision. Residual nuclei distributions produced in thick targets by high-energy cascades are often of interest in evaluating the radiation hazards around high-energy accelerators[13,14] and in studying the effects of cosmic-ray bombardment.[15,16]

Since the introduction of the scaling model, the high-energy intranuclear-cascade code (HECC)[17] has become available and can now be used to generate this inelastic collision data. This model (HECC), in addition to containing the effects of a diffuse nuclear surface, the Fermi motion of the bound nucleons within the nucleus, the exclusion principle applied to the zero-temperature Fermi gas model, and a local potential for nucleons (as did MECC), also

†It has been found by Gabriel and Santoro[13] that the energy system of emitted particles predicted by the extrapolation method compares more favorably with experimental data if special provisions are made in scaling those particles emitted as a result of "quasi-elastic" scattering collisions inside the nucleus. These special provisions are retained in the version of the extrapolation method used in HETC.

takes into account a localized reduction in the density of the nucleus during the development of the particle cascade. The high-energy nucleon-nucleon and pion-nucleon production of pions within the nucleus is taken into account via phenomenological fits to experimental data mentioned earlier. These fits include the increase in particle multiplicity with increasing incident energy.[8] A complete incorporation of this model (HECC) into HETC will not be completed until a much later date. Until then, data generated by HECC for selected nuclides (Fe, C) at energies of 5, 10, 20, 40, 80, and 160 GeV for incident neutrons, protons, and charged pions have been placed in a data base for use by HETC. The scaling model is used to fill in all intermediate energies above ~3 GeV.

An Application Using HETC

HETC is an integral part of the CALOR[18] computer system which is used to determine the response of calorimeters to high-energy hadrons and leptons. The coupling of HETC and the other codes (EGS, MORSE, and SPECT) is illustrated in Fig. 2. A calorimeter that has been recently analyzed by CALOR is described in Table 1.

Table 1

Calorimeter Configurations from Upstream to Downstream of Beam

Counter	Thickness (cm)	Material
A	1.27	Plastic Scintillator
	5.08	Pb
	15.24	Fe
B	1.27	Plastic Scintillator
	3.81	Fe
C	1.27	Plastic Scintillator
	30.48	Fe
E	1.27	Plastic Scintillator
D	7.62	Liquid Scintillator

The energy deposited in each counter was recorded for every cascade simulated. In order to compare the results of the simulation with data, energy deposited in the plastic scintillator which has been corrected for saturation effects must be converted to equivalent particles. An equivalent particle was defined as the median of the signal distribution in each counter due to 3.5-GeV/c muons going through the calorimeter. The average of each Landau distribution was set equal to the average energy loss of the particle crossing (or stopping in) the plastic

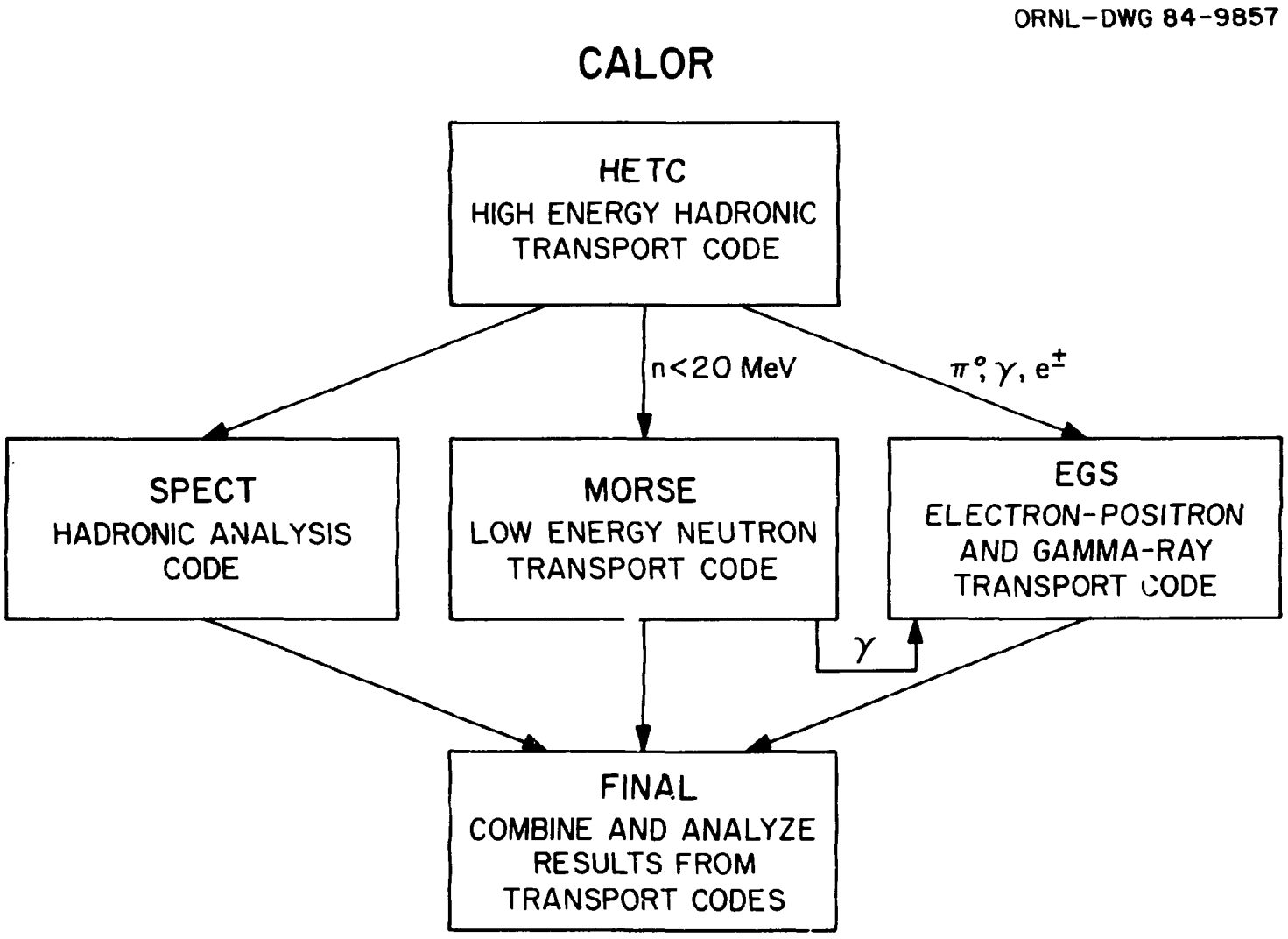

Fig. 2. Flow diagram of the CALOR system.

scintillator as calculated using the restricted energy loss formula and adding the energy deposited by knock-on electrons from the absorber upstream of each counter (approximately 0.4 MeV for the 1.27 cm detectors, and 1.6 MeV for the 7.6 cm detector). The result is that an equivalent particle corresponds to approximately 2.2 ± .2 MeV for the 1.27 cm counters and 11.9 ± 1.2 MeV for the liquid counter. This energy conversion is used to compare the simulation with data.

In Table 2 the average ($\overline{X}$) and standard deviation (σ) of the signal distribution for data and simulation are presented. The two agree to within the accuracy of the conversion to equivalent particles. Figure 3 shows the distribution of signals in the various counters for data and simulation. There is again no disagreement between data and simulation to within the accuracy of the conversions.

Table 2
Average ($\overline{X}$) and Width (σ) of Signal in Equivalent Particles of BNL Experiment and ORNL Simulation

Particle Momentum	Counter B		Counter C		Counter E		Counter D	
	$\overline{X}$	σ	$\overline{X}$	σ	$\overline{X}$	σ	$\overline{X}$	σ
3.5 GeV/c								
BNL	3.38 ± .08	6.4	2.77 ± .07	5.8	0.69 ± .03	2.8	0.38 ± .02	1.3
ORNL	2.9 ± .1	4.9	2.7 ± .1	4.7	0.58 ± .04	1.9	0.57 ± .04	1.6
10 GeV/c								
BNL	10.6 ± .2	13.2	9.5 ± .2	12.4	3.0 ± .1	7.0	1.76 ± .06	4.0
ORNL	9.7 ± .2	11.0	9.1 ± .2	10.7	3.5 ± .2	7.3	2.9 ± .1	4.7

The mechanisms producing the observed signals can be studied further by looking at correlations between counter pairs. Counter correlations have been quantified using the correlation matrix. M_{AB}, the matrix element for counters A and B, is defined by

$$M_{AB} = \frac{\sum_{i=1}^{N} (A_i - \overline{A})(B_i - \overline{B})}{\left[\sum_{i=1}^{N} (A_i - \overline{A})^2 \sum_{i=1}^{N} (B_i - \overline{B})^2 \right]^{1/2}},$$

where A_i and B_i are the pulse heights in counters A and B for event i, $\overline{A}$ and $\overline{B}$ are the average signals in the two counters and N is the total number of events. M equals one for perfect correlation, zero for no correlation, and minus one for perfect anticorrelation. The matrix is compared for data and simulation in Table 3.

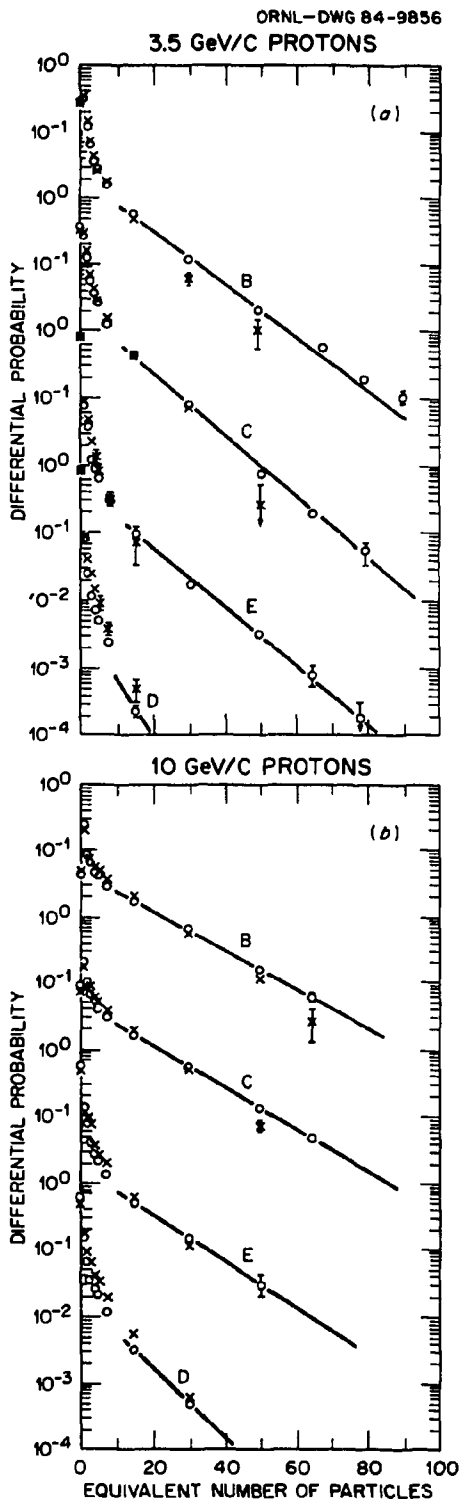

Fig. 3. Pulse height in equivalent particles for one of the four detectors in the calorimeter for data (circles) and simulation (crosses). Error bars are statistical and where none are shown they are of comparable size or smaller than the symbol used.

Another calorimeter consisting of 49 iron plates ranging in thickness from 3.8 to 10.1 cm and 3.2-cm liquid scintillator counters was used in a Fermi National Accelerator Laboratory (FNAL) experiment by Bodek et al.[19] Calorimeter calibration data were recorded for incident protons of 50 and 100 GeV and pions of 278 GeV.

Table 3

Comparison of BNL and ORNL Correlation Matrix

Particle Momentum	BNL Counter				ORNL Counter			
	B	C	E	D	B	C	E	D
				3.5 GeV/c				
B	1.0	0.15	-0.06	-0.06	1.0	0.17	-0.04	-0.06
C		1.0	-0.03	-0.03		1.0	-0.01	-0.02
E			1.0	0.46			1.0	0.59
D				1.0				1.0
				10 GeV/c				
B	1.0	0.39	-0.17	-0.19	1.0	0.40	-0.18	-0.22
C		1.0	-0.13	-0.15		1.0	-0.15	-0.18
E			1.0	0.71			1.0	0.72
D				1.0				1.0

Two detectors in that calorimeter are at approximately the same depth as the B and C counters of this calorimeter and are separated from each other by an identical thickness of absorber. The summed pulse heights of these two detectors are compared with the sum of the B and C counters for 50- and 100-GeV/c cases in Fig. 4. Because of trigger requirements imposed in the FNAL calorimeter, the distributions are normalized at 100 equivalent particles.

The fraction of the summed pulse height in the C layer relative to B+C is compared for experimental and simulation data in Fig. 5a-c for 50- to 200-GeV/c incident protons. The simulation thus successfully predicts both individual counter responses and two counter correlations quite successfully even at high energies.

Since HETC is the driving force determining the results of these calculations and since these results indicate fairly good agreement with experimental data, it must be concluded that the physics in HETC is not totally out of line with reality. However, as with any code, additional improvement and updating is always possible.

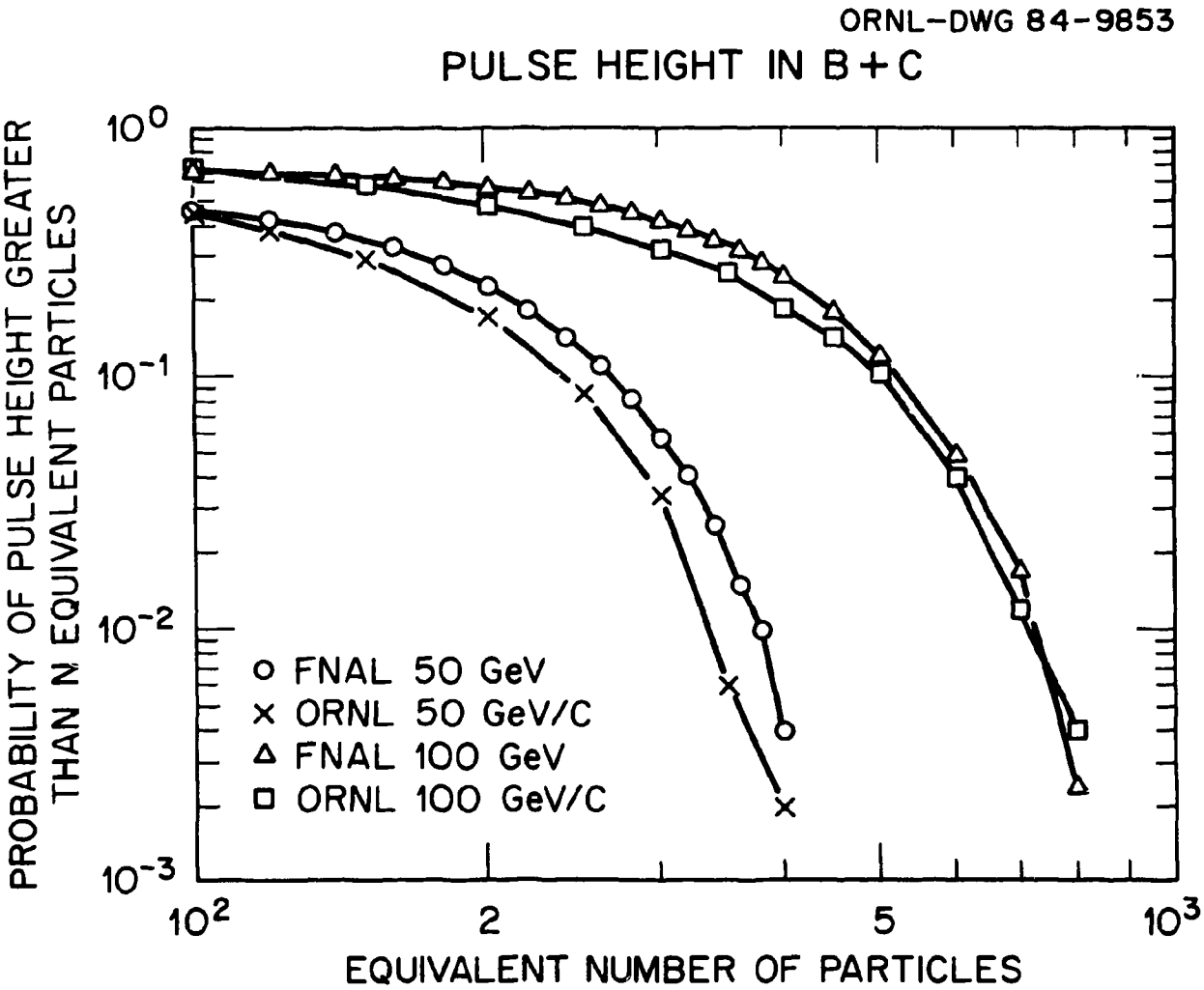

Fig. 4. The simulated pulse height distribution in the summed B and C layers is compared with data from a similar but not identical calorimeter. The probability of getting a pulse height greater than X equivalent particles is shown, with data normalized to the simulated value at 100 equivalent particles.

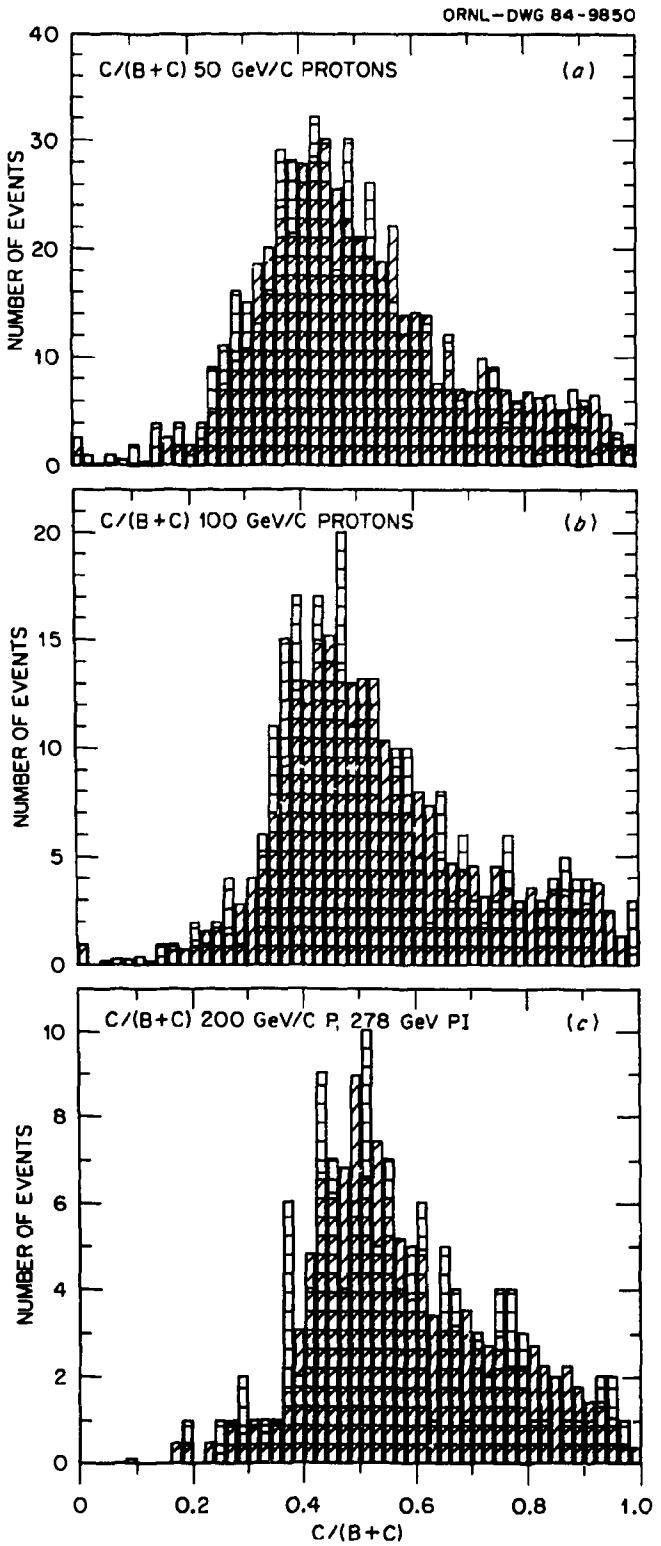

Fig. 5. Correlations between the C and B counters in simulated events (horizontal lines) are compared with data (diagonal lines) by plotting the ratio of the pulse height in the C counter to the sum of the B and C counters.

REFERENCES

1. K. C. Chandler and T. W. Armstrong, "Operating Instructions for the High-Energy Nucleon-Meson Transport Code, HETC," ORNL-4744, Oak Ridge National Laboratory, Oak Ridge, TN (1972).
2. R. L. Ford and W. R. Nelson, "The EGS Code System Computer Program for the Monte Carlo Simulation of Electromagnetic Cascade Showers (Version 3)," SLAC Report No. 210, Stanford Linear Accelerator Center, Stanford, CA (1978).
3. B. Rossi, *High-Energy Particles*, Prentice-Hall, Inc., Englewood Cliffs, NJ (1952).
4. T. W. Armstrong and R. G. Alsmiller, Jr., *Nucl. Instr. Methods* **82**, 289 (1970).
5. W. A. Coleman, "Thermal-Neutron Flux Generation by High-Energy Protons," ORNL/TM-2206, Oak Ridge National Laboratory, Oak Ridge, TN (1968).
6. W. E. Kinney, "The Nucleon Transport Code, NTC," ORNL-3610, Oak Ridge National Laboratory, Oak Ridge, TN (1964).
7. M. P. Guthrie et al., *Nucl. Instrum. Methods* **66**, 29 (1968), and M. P. Guthrie et al., *Nucl. Instrum. Methods* **91**, 669 (1971).
8. T. A. Gabriel, R. T. Santoro, and J. Barish, "A Calculational Method for Predicting Particle Spectra from High-Energy Nucleon and Pion Collisions ($\geq$ 3 GeV) with Protons," ORNL/TM-3615, Oak Ridge National Laboratory, Oak Ridge, TN (1971), and J. Ranft and T. Borek, "Improved Nucleon-Meson Cascade Calculations," FN-193, 1100.0, Fermi National Accelerator Laboratory, Batavia, IL (1970).
9. R. M. Sternheimer and S. J Lindenbaum, *Phys. Rev.* **123**, 333 (1961); *Phys. Rev.* **109**, 1723 (1958); *Phys. Rev.*, **105**, 1874 (1957).
10. H. W. Bertini and M. P. Guthrie, *Nucl. Phys.* **A169**, 670 (1971), and M. P. Guthrie, "EVAP-4: Another Modification of a Code to Calculate Particle Evaporation from Excited Compound Nuclei," ORNL/TM-3119, Oak Ridge National Laboratory, Oak Ridge, TN (1970).
11. R. Hofstadter, *Rev. Mod. Phys.* **28**, 214 (1956).
12. T. A. Gabriel, R. G. Alsmiller, Jr., and M. P. Guthrie, "An Extrapolation Method for Predicting Nucleon and Pion Differential Production Cross Sections from High-Energy (> 3 GeV) Nucleon-Nucleus Collisions," ORNL-4542, Oak Ridge National Laboratory, Oak Ridge, TN (1970).
13. T. A. Gabriel and R. T. Santoro, *Nucl. Instrum. Methods* **95**, 275 (1971).
14. R. G. Alsmiller, Jr. and J. Barish, *Nucl. Instrum. Methods* **36**, 309 (1965).
15. T. W. Armstrong and R. G. Alsmiller, Jr., *Proc. Apollo 12 Lunar Science Conference, Geochim. Cosmochim. Acta* **2**, Suppl. 2, 1729-1745, M.I.T. Press (1971).
16. T. W. Armstrong and K. C. Chandler, "Calculation of the Dose, Radionuclide Production, and Delayed Photon Leakage Due to Solar-Proton Bombardment of Tissue with Application to Astronaut Dosimetry," ORNL/TM-3452, Oak Ridge National Laboratory, Oak Ridge, TN (1971).

17. H. W. Bertini et al., *Phys. Rev.* C17, 1382 (1978).

18. T. A. Gabriel et al., "A Monte Carlo Simulation of the Response of a Hadronic Calorimeter to Protons of Momentum 3.5 to 200 GeV/c," ORNL/TM-9270, Oak Ridge National Laboratory, Oak Ridge, TN (1985).

19. A. Bodek and J. L. Ritchie, Fermi National Accelerator Laboratory, private communication, 1984.

INTERNAL DISTRIBUTION

1. L. S. Abbott
2. F. S. Alsmiller
3. R. G. Alsmiller, Jr.
4. D. E. Bartine
5–9. B. L. Bishop
10–14. T. A. Gabriel
15. R. A. Lillie
16. F. C. Maienschein
17. R. W. Peelle
18. RSIC
19. R. T. Santoro
20. A. Zucker
21. P. W. Dickson, Jr. (Consultant)
22. G. H. Golub (Consultant)
23. D. Steiner (Consultant)
24–25. Central Research Library
26. ORNL Y-12 Technical Library Document Reference Section
27–28. Laboratory Records
29. ORNL Patent Office
30. Laboratory Records - RC

EXTERNAL DISTRIBUTION

31. Office of Assistant Manager for Energy Research & Development, DOE-ORO, Oak Ridge, TN 37830

32. Argonne National Laboratory, Library Services Department, 302-CE125, 9700 S. Cass Avenue, Argonne, IL 60439

33. T. W. Armstrong, Science Applications, Inc., PO Box 2807, La Jolla, CA 92038

34. Miguel Awschalom, National Accelerator Laboratory, PO Box 500, Batavia, IL 60510

35. V. S. Barashenkov, Laboratory of Theoretical Physics, Joint Institute for Nuclear Research, Head Post Office, PO Box 79, Moscow, USSR

36. Dr. Gerald W. Bennett, Brookhaven National Laboratory, Upton, NY 11973

37. D. Berley, National Science Foundation, Washington, DC 20550

38. Dr. Elliott Bloom, Stanford Linear Accelerator Center, PO Box 4349, Stanford, CA 94305

39. J. Brau, University of Tennessee, Dept. of Physics, Knoxville, TN 37919

40. Dr. Bruce Brown, Fermi National Accelerator Laboratory, PO Box 500, Batavia, IL 60510

41. Dr. David O. Caldwell, Department of Physics, Univ[illegible]y of California at Santa Barbara, Santa Barbara, CA 93106

42. Stanley B. Curtis, Lawrence Radiation Laboratory, Bldg. 29, Room 213, Berkeley, CA 94720

43. Herbert Destaebler, Stanford Linear Accelerator Center, Stanford University, Stanford, CA 94305

44. R. D. Edge, Physics Department, University of South Carolina, Columbia, SC 29208

45. Dr. R. Eisenstein, Department of Physics, University of Illinois, Urb[illegible]a, IL 61801

46. R. W. Ellsworth, George Mason University, Fairfax, VA 22030

47. Dr. Chris Fabjan, CERN, Geneva 23, Switzerland

48. Dr. G. Feldman, Stanford Linear Accelerator Center, Stanford University, Stanford, CA 94305

49. Dr. W. T. Ford, Experiment lA-Lab C, Fermi National Accelerator Laboratory, PO Box 500, Batavia, IL 60510

50. Dr. E. Fowler, Department of Physics, Purdue University, West Lafayette, IN 47907

51. H. T. Freudenreich, University of Maryland, College Park, MD 20742

52. E. Freytag, Deutsches Elektronen-Synchrotron, DESY, 2 Hamburg Dr., Flottbek, Notkesteig l, W. Germany

53. Dr. G. T. Gillies, Department of Physics, University of Virginia, Charlottesville, VA 22901

54. Dr. Gary E. Gladding, University of Illinois, Department of Physics, Urbana, IL 61801

55. K. Goebel, Health Physics Group, CERN, 1211 Geneva 23, Switzerland

56. J. A. Goodman, University of Maryland, College Park, MD 20742

57. Dr. M. Goodman, Department of Physics, Harvard University, Cambridge, MA 02138

58. Dr. Herman Grunder, Deputy Director, General Sciences, Lawrence Berkeley Laboratory, Bldg. 50A, Room 4119, 1 Cyclotron Rd., Berkeley, CA 94720

59. H. J. Hargis, University of Tennessee, Department of Physics, Knoxville, TN 37919

60. Frenc Hajnal, Health and Safety Laboratory, U.S. Department of Energy, 376 Hudson St., NY, NY 10014

61. M. Hofert, CERN, 1211 Geneva 23, Switzerland

62. Mr. Terrence Jensen, Dept. of Physics and Astronomy, The University of Rochester, Rochester, NY 14627

63. Prof. D. Lal, Tata Institute of Fundamental Research, National Centre of the Government of India for Nuclear Science & Mathematics, Homi Bhabha Rd., Bombay 5, India

64. Lawrence Livermore Laboratory, Technical Information Department, PO box 808, Livermore, CA 94550

65. V. Lebedev, Institute of High Energy Physics, Serpukhov, Moscow Region, USSR

66. Library for Nuclear Science, Massachusetts Institute of Technology at Middleton, Middleton, MA 01949

67. Dr. J. LoSecco, Department of Physics, California Institute of Technology, Pasadena, CA 91125

68. Dr. J. Marks, Accelerator Fusion Research Division, Lawrence Berkeley Laboratory, Bldg. 50, Room 149, 1 Cyclotron Rd., Berkeley, CA 94720

69. A. I. Mincer, University of Maryland, College Park, MD 20742

70. Dr. V. S. Narasimham, Tata Institute of Fundamental Research, Bombay 400 005, India

71. W. R. Nelson, Stanford Linear Accelerator Center, Stanford University, PO Box 4349, Stanford, CA 94305

72. Keran O'Brien, Health and Safety Laboratory, U.S. Department of Energy, 376 Hudson St., NY, NY 10014

73. Dr. T. R. Palfrey, Jr., Department of Physics, Purdue University, West Lafayette, IN 47907

74. Dr. Robert Palmer, Brookhaven National Laboratory, Upton, NY 11973

75. Dr. C. W. Peck, Department of Physics, California Institute of Technology, Pasadena, CA 91109

76. J. Ranft, Karl-Marx University, Physics Section, Linnestrasse 5, 701 Leipzig, W. Germany

77. Dr. Lincoln Reed, Division of High Energy and Nuclear Physics, Department of Energy, Washington, DC 20545

78. Dr. C. Rubbia, Lyman Laboratory, Harvard University, Cambridge, MA 02138

79. Dr. W. Schmidt, Institute of Experimental Nuclear Physics, University of Karlsruhe, 75 Karlsruhe, W. Germany

80. The Secretary, Radiation Group, Lab II, CERN, 1211 Geneva 23, Switzerland

81. Dr. Walter Selove, University of Pennsylvania, Department of Physics, Philadelphia, PA 19104

82. B. S. P. Shen, Department of Astronomy, University of Pennsylvania, Philadelphia, PA 19104

83. Dr. M. Shupe, Department of Physics, University of Minnesota, Minneapolis, MN 55455

84. Stanford Linear Accelerator Center, Attention: Library, PO Box 4349, Stanford, CA 94305

85. Dr. Alan Stevens, Physics Department, Brookhaven National Laboratory, Upton, NY 11973

86. G. R. Stevenson, Radiation Protection Group, Lab II, CERN, 1211 Geneva 23, Switzerland

87. Dr. L. Sulak, Department of Physics, University of Michigan, Ann Arbor, MI 48109

88. R. F. Taschek, Los Alamos National Laboratory, P.O. Box 1663, Los Alamos, NM 87544

89. R. Tesch, DESY, Hamburg, Notkesteig 1, W. Germany

90. Ralph H. Thomas, University of California, Lawrence Radiation Laboratory, Health Physics Department, Bldg.72, Berkeley, CA 94720

91. V. D. Toneev, Laboratory of Theoretical Physics, Joint Institute for Nuclear Research, Head Post Office, PO Box 79, Moscow, USSR

92. S. C. Tonwar, University of Maryland, College Park, MD 20742

93. W. Turchinetz, Massachusetts Institute of Technology, R26-411, Cambridge, MA 02139

94. Dr. W. J. Willis, CERN, Geneva 23, Switzerland

95. Dr. D. Winn, Lyman Laboratory, Harvard University, Cambridge, MA 02138

96. Dr. J. Wilcznski, Nuclear Research Center, Karlsruhe, W. Germany

97. Dr. S. Yellin, Stanford University, Stanford Linear Accelerator Center, P.O. Box 4349, Stanford, CA 94305

98. G. B. Yodh, University of Maryland, College Park, MD 20742

99. Dr. B. Zeitnitz, Nuclear Research Center, Karlsruhe, W. Germany

100–126. Technical Information Center, PO Box 62, Oak Ridge,TN 37831